ARCHIVIO ISTITUZIONALE DELLA RICERCA

Alma Mater Studiorum Università di Bologna
Archivio istituzionale della ricerca

Electrical characteristics of HTS coils with and without insulation in a layer-wound configuration

This is the final peer-reviewed author's accepted manuscript (postprint) of the following publication:

Published Version:
Andrea Musso, G.A. (2021). Electrical characteristics of HTS coils with and without insulation in a layer-wound configuration. IEEE TRANSACTIONS ON APPLIED SUPERCONDUCTIVITY, 31(5), 1-5 [10.1109/TASC.2021.3059971].

Availability:
This version is available at: https://hdl.handle.net/11585/817001 since: 2022-11-07

Published:

DOI: http://doi.org/10.1109/TASC.2021.3059971

Terms of use:

Some rights reserved. The terms and conditions for the reuse of this version of the manuscript are specified in the publishing policy. For all terms of use and more information see the publisher's website.

This item was downloaded from IRIS Università di Bologna (https://cris.unibo.it/).
When citing, please refer to the published version.

(Article begins on next page)

17 December 2025

This is the final peer-reviewed accepted manuscript of:

A. Musso et al.

Electrical Characteristics of HTS Coils With and Without Insulation in a Layer-Wound Configuration

In: *IEEE Transactions on Applied Superconductivity, vol. 31, no. 5, pp. 1-5, Aug. 2021*

The final published version is available online at:

https://doi.org/10.1109/TASC.2021.3059971

Rights / License:

The terms and conditions for the reuse of this version of the manuscript are specified in the publishing policy. For all terms of use and more information see the publisher's website.

This item was downloaded from IRIS Università di Bologna (https://cris.unibo.it/)

When citing, please refer to the published version.

Electrical characteristics of HTS coils with and without insulation in a layer-wound configuration

A. Musso, G. Angeli, M. Ascade, M. Bocchi, P. L. Ribani, V. Rossi, A. Valzasina and M. Breschi

***Abstract* —This paper analyses the current distribution in no-insulation (NI) coils in a layer-wound configuration. The investigation aims at comparing the electrical characteristic of two coils wound from the same BSCCO tape, with or without electrical insulation between turns. Both coils are characterized by a very similar geometry, with the same number of turns and layers. Both coils, cooled in liquid nitrogen bath, are charged until the tape critical current is exceeded. To interpret the measurements and analyze the current distribution within the winding, a lumped-parameter equivalent electrical circuit is developed and solved numerically in a time-varying regime. The model results are compared with the signals acquired through voltage taps soldered at the same locations in both coils. Finally, the model is applied to investigate the impact of the transverse contact resistance and to estimate the most stressed locations of the coil during charging, in terms of power produced by Joule effect.**

***Index Terms* — No-insulation coils, Superconducting coils, Layer-wound technique, Current distribution, High Temperature Superconductors.**

I. Introduction

A possible solution to the quench protection issues occurring in HTS devices is offered by the use of NI coils, wound without electrical insulation between turns [1]. In these coils, the current can flow in the radial direction and avoid the damaged/quenched areas, thus improving the overall thermal stability [2 – 5]. However, transverse currents flowing in radial direction can also arise in the absence of quenches, which is not desirable in most applications. In general, superconducting coils are designed to operate with the same current along each turn, which allows generating the design magnetic field. It is therefore important to establish the operating conditions at which these currents arise and to determine their intensity.

The NI coils are usually realized either with the pancake-wound technique or with the layer-wound one [6]. In pancake coils, the turns are in radial contact with adjacent layers, which are relatively close to each other along the tape length. In layer-wound coils instead, a turn can be in contact with adjacent turns that are rather distant from each other along the tape length, depending on their specific location inside each layer. The two types of winding result in different current distributions during electrodynamic transients, which requires to analyze separately these two techniques. The layer-wound technique is selected for this work, since this is not investigated extensively in the literature for NI coils [7 – 11], differently from the pancake-wound technique [12 – 19]. Moreover, in this configuration the number of superconducting joints can be reduced [8, 20].

In this work, measurements of the *V-I* electrical characteristic were carried out on two windings, with and without insulation, of almost identical geometry. To interpret the experimental results obtained, with special reference to the peculiar behavior of the voltages recorded across different layers of the winding, this paper proposes an electrodynamic model based on a non -linear lumped parameter circuit of the coil. The model results are compared to the experimental ones, thus giving an insight in the distribution of current and dissipated power inside the winding.

II. Experimental Setup

Two coils are realized using the layer-wound technique, with and without insulation. The coils are wound on two identical mandrels, with the same number of layers (N_L) and turns per layer (N_T). The mandrel outer diameter (82 mm) is selected so as not to degrade the tape critical current due to bending [21]. The main coil parameters are presented in Table I.

TABLE I
Tape and Coil Parameters

Tape thickness [μm]	300.0
Tape width [mm]	4.1
Inner radius [mm]	41.0
Number of layers (N_L)	3
Number of turns per layer (N_T)	10
Insulated coil / NI coil	
Length of each layer [cm]	258.8 / 259.1 ; 260.6 / 261.4 ; 262.5 / 263.6
I_c *of each layer* [A]	109.5 / 109.5 ; 109.5 / 109.5 ; 113.4 / 109.5
n-value of all layers	13.5 / 13.5

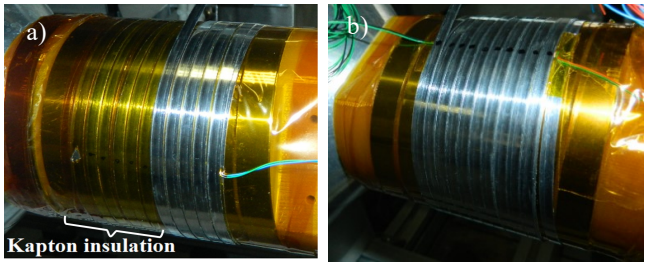

Fig. 1. Winding phase for the (a) insulated and (b) NI coils.

A. Musso, M. Breschi and P. L. Ribani are with the Department of Electrical, Electronic and Information Engineering, of the University of Bologna, 40136 Bologna, Italy (e-mail: andrea.musso3@unibo.it).

G. Angeli, M. Ascade, M. Bocchi, V. Rossi and A. Valzasina are with RSE S.p.A., 20134 Milan, Italy.

Color versions of one or more of the figures in this paper are available online at http://ieeexplore.ieee.org.

Template version 8.0d, 22 August 2017. IEEE will put copyright information in this area
See http://www.ieee.org/publications_standards/publications/rights/index.html for more information.

A *High Strength Plus* BSCCO tape manufactured by *American Superconductor Corp.* [22], cut from the same lot is used to wind both coils. In the NI coil, the layers are wound on top of each other without inserting any insulation. In the insulated coil, each layer is separated from the adjacent ones by a Kapton layer of 50 μm thickness, positioned during the winding phase. This creates a difference between the outer radius of the two coils (41.9 mm and 42.1 mm for the insulated and the NI coils, respectively), which however can be considered negligible. In the NI coil, a minimum pitch is kept to avoid uninsulated electrical contacts between turns of the same layer. Fig. 1 shows two photos taken during the winding phase of the coils. Both coils are instrumented with voltage taps soldered on the tape surface at the ends of each layer. No voltage taps are introduced between the layers to avoid deforming the winding.

Each winding is connected to a DC power supply, which can generate both current ramps and step profiles of variable amplitude and duration. The tests on both coils are carried out in a liquid nitrogen bath, charging each coil up to 130 A with a ramp-rate of 1 A/s.

III. EQUIVALENT ELECTRIC CIRCUIT

The electrical characteristics of the layer-wound coils is analyzed through the equivalent lumped parameter circuit presented in Fig. 2.

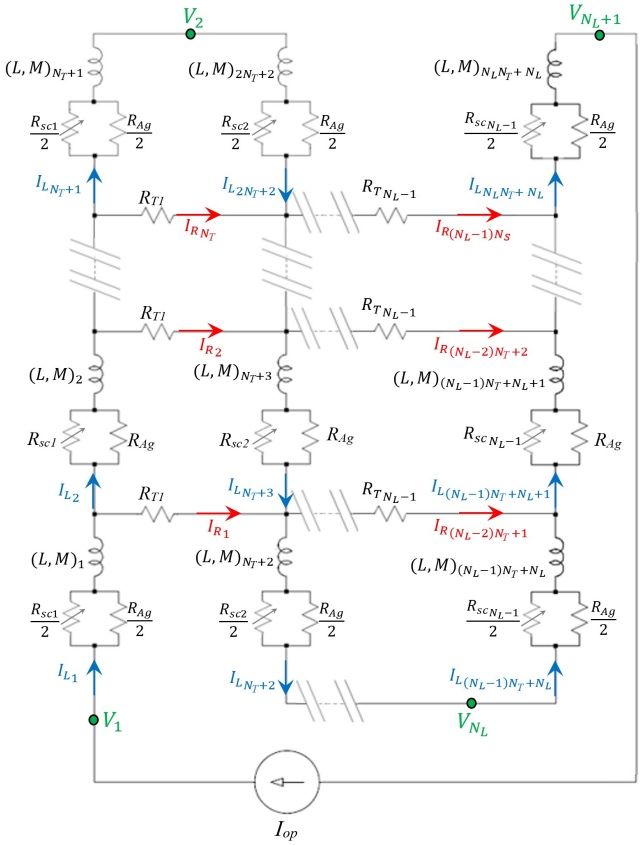

Fig. 2. Equivalent non-linear lumped parameters electric circuit of a layer-wound coil with a generic number of turns and layers.

The double bars indicate that the circuit branches can be replicated for a generic number of layers and turns.

The current source imposing the operation current (I_{op}) is connected to the first turn of the inner layer and to the last turn of the outer layer of the coil. In the circuit, each half turn of the winding is represented as the series between a linear inductor and a non-linear resistor. The terms $(L,M)_i$ correspond to the self-inductances of each longitudinal branch and the mutual-inductances between each other. To better reproduce the BSCCO tape, each longitudinal resistor is given by the parallel connection between the non-linear resistance of the superconductor ($R_{sc,i}$) and the linear resistance of the silver matrix (R_{Ag}). The power law is adopted for the superconductor electric characteristics [23]. The resistivity of silver at 77 K is taken equal to 2.7 nΩ · m [24] and the fill-factor of the tape is set to 30%. To consider the possible inhomogeneity of the superconductor, the critical current and the *n-value* can be varied between the layers.

To account for the current flowing radially between layers, transversal resistances ($R_{T,i}$) are introduced. By varying these parameters, it is possible to include the presence of an electrical insulation. Each turn is considered to be in contact with the turns of the adjacent layers at its same height (*i.e.* on the left and right sides) by means of a resistance $R_{T,i}$ which is lumped in the middle of the turn length. Therefore, it is assumed that all layers perfectly overlap at the same height. This approximation neglects the different winding angle of each layer, due to which the turns that can be in direct contact with only one turn of the adjacent layer.

Lumping the transversal resistances in the middle of each turn allows one reducing the number of elements in the circuit. Since there are no branches connected between the second half of a turn and the first half of the subsequent turn, their longitudinal resistances and inductances are in series and can be represented as a single electric component. The electric components representing the first and last half turns of each layer are instead kept separate, in order to keep the various layers distinct in the circuit representation. Thus, the corresponding resistances and inductances are halved with respect to those of the other branches of the same layer. Each layer is therefore described with N_T+1 longitudinal branches, each connected to the previous or subsequent layer with N_T transverse branches.

The transverse contacts between turns belonging to the same layer (*i.e.* along their thickness) is assumed negligible.

The currents flowing in the longitudinal ($I_{L,i}$) and transverse ($I_{R,i}$) branches are highlighted in Fig. 2 with different labels, colors and the corresponding numbering. For a coil with a generic number of turns and layers, the number of longitudinal currents is $(N_T+1)\cdot N_L$, while the number of transverse currents is $(N_L-1)\cdot N_T$. The positive reference direction of the longitudinal currents is in agreement with the path followed by the tape during the winding phase. In the first layer, the positive orientation is directed from bottom to top, and is then inverted at each subsequent layer. The positive direction of the transverse currents is taken from left to right.

The loop analysis is adopted to solve the circuit [25]. The number of problem unknowns, namely the loop currents, is

equal to $N_L \cdot N_T$. Once the system is solved, the branch currents can be computed as the algebraic sums of the currents of the loops adjacent to the branch considered. Since I_{op} can vary in time, a system of differential equations has to be solved. The numerical method adopted to solve this system is the Cash-Karp Embedded Runge-Kutta of 5th order [26].

Finally, from the branch currents it is possible to compute the voltage differences between each pair of nodes of the circuit. The green dots in Fig. 2 represent the locations of the N_L+1 voltage taps inserted in the coils, from which the values of the average electric fields are computed, dividing by the length of each layer.

IV. RESULTS AND DISCUSSIONS

A. *Electric field profiles and current distribution*

The measured electric characteristics of the insulated and NI coils are plotted in Fig. 3a and Fig. 3b respectively. For the insulated coil, the different profile of the 3rd layer as compared to the others is ascribed to a higher I_c value of the tape in this layer, as reported in Table I. The discrepancy (3.5%, as compared to the other layers), is due to a non-uniformity of the tape, and can be considered as acceptable.

In the simulations with the equivalent circuit, both resistances between the turns of the 1st and the 2nd layers ($R_{T,1}$) and the turns of the 2nd and the 3rd layers ($R_{T,2}$) are set to 30.0 mΩ. It was verified that this is the minimum value that guarantees obtaining transverse currents of negligible amplitude. If a lower value is selected, the difference between the voltage curves increases and the coil electrical behavior gradually shifts towards that of a NI one.

The NI coil exhibits a peculiar behavior, since the electric fields in the first and the last layers exhibit a practically identical growth, while that in the central layer increases more slowly. In particular, the electric field in the 3 layers remains the same up to $I_{op} < 0.8 \cdot I_c$, while for higher amplitudes, the curves diverge. The experimental curves can be well reproduced with the numerical model, by using the transverse resistances between layers as fitting parameters. In particular, the resistance $R_{T,1}$ between layers 1 and 2 is set to 2.0 mΩ while $R_{T,2}$ between layers 2 and 3 is set to 0.5 mΩ. This non-uniformity of the contact between layers could be due to the winding phase, where a different tensional state could have been applied to the tape. The different simulated behavior of the outer layers is related to the different values of $R_{T,1}$ and $R_{T,2}$; it was verified, by setting these two parameters equal, that the outer layers exhibit the same *V-I* curve.

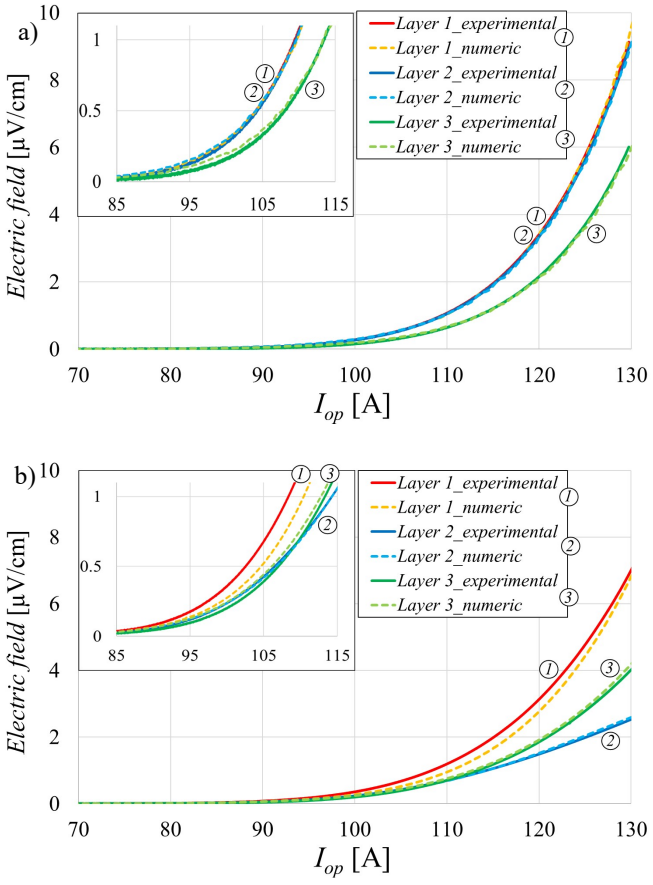

Fig. 3. Comparison of the electric field measured during tests and computed numerically for the 3 layers of the (a) insulated and (b) NI coils. The insets magnify the curves up to 1 μV/cm (corresponding to the critical field).

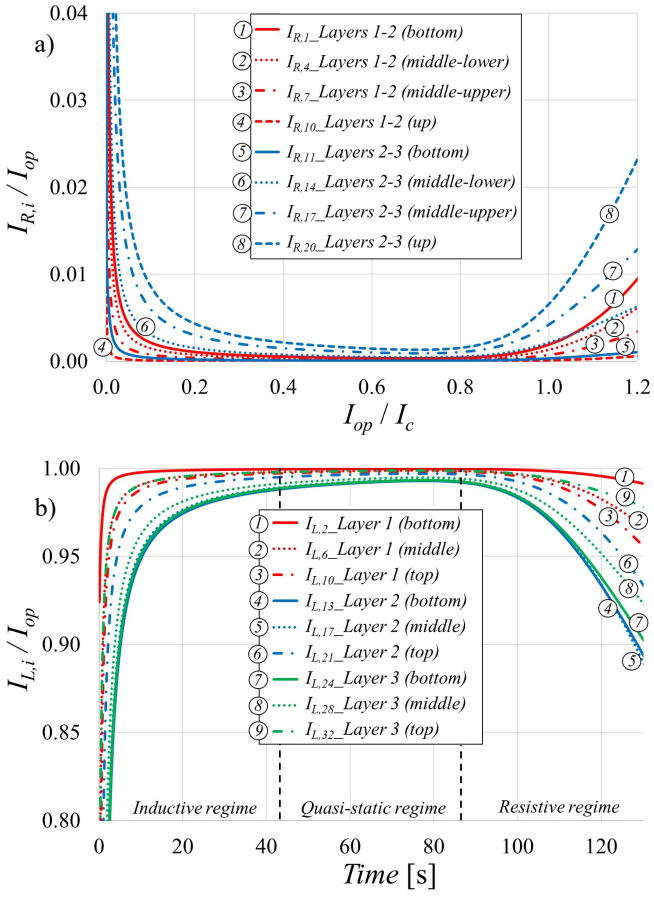

Fig. 4. (a) Longitudinal and (b) transverse currents flowing in selected branches of the equivalent circuit during the charging phase of the NI coil.

Fig. 4a presents the ratio between the longitudinal currents and I_{op}, in 3 branches of each layer of the NI coil, located at the same height ($I_{L,2}$, $I_{L,13}$ and $I_{L,24}$ at the bottom, $I_{L,6}$, $I_{L,17}$ and $I_{L,28}$ in the middle, $I_{L,10}$, $I_{L,21}$ and $I_{L,32}$ at the top) during the coil energization (expressed as the ratio with I_c). Fig. 4b shows the ratio between the transverse currents and I_{op}, in 4 branches between each pair of layers of the coil, located at the same height ($I_{R,1}$ and $I_{R,11}$ at the bottom, $I_{R,4}$ and $I_{R,14}$ in the middle-lower part, $I_{R,7}$ and $I_{R,17}$ in the middle-upper part, $I_{R,10}$ and $I_{R,20}$ at the top) during the coil charging. At $I_{op}/I_c < 0.4$, the current distribution is mainly driven by the inductances of the circuit (*inductive regime*). The time constants of this electrodynamic transient range from 5 s to 50 s. During the transient, the current in each branch evolves differently, depending on its location in the circuit. At $0.4 < I_{op}/I_c < 0.8$, an almost steady-state condition is reached (*quasi-static regime*), in which all the longitudinal branches are almost evenly loaded. At $I_{op}/I_c > 0.8$, the longitudinal currents start to spread again due to the transition from superconducting to normal state (*resistive regime*). This is particularly evident for the longitudinal branches located in the 2nd and 3rd layers, in the middle-lower section of the circuit. At $I_{op}/I_c = 1.2$, the current flowing in these branches is about 88% of I_{op}; correspondingly, a certain amount of current flows in the transverse paths. The transverse currents start to rise at $I_{op}/I_c > 0.8$, reaching a maximum amplitude about 2.4% of I_{op} when $I_{op}/I_c = 1.2$. The transverse currents are greater between the 2nd and 3rd layers since $R_{T,2} < R_{T,1}$, while they are smaller at the bottom of the coil between the 2nd and 3rd layer, and at the top of the coil between the 1st and 2nd layer.

It can be concluded that the NI coil is not loaded uniformly during the energization. For the ramp-rate used in this work, the inhomogeneity due to the resistive transition occurs when I_{op} exceeds amplitudes higher than the safety margin usually adopted for a superconducting device, generally not greater than 80% of I_c [27 – 29]. If the resistances $R_{T,i}$ are lowered, the threshold at which the longitudinal currents become inhomogeneous due to the resistive transition is reduced.

B. *Dissipated power distribution*

Once the branch currents of the equivalent circuit are computed, the power dissipated by Joule effect in each branch can be determined as $R \cdot I^2$, where R is the branch resistance (longitudinal or transverse). Then, it is interesting to evaluate the heat generated in each turn of the winding. Since each longitudinal branch represents either half turn or the sum of two half turns, half of the power generated by two consecutive longitudinal branches is assigned to each turn (or the whole power, if the branches are the first or the last of a given layer, see Fig. 2). As for the power dissipated in the transverse branches, this is equally subdivided between the two longitudinal branches it connects. At the end of the process, the heat generated in the $N_L \cdot N_T$ turns of the winding is retrieved.

Fig. 5 shows the dissipated power distribution within the NI coil during the charging phase, at (a) $I_{op}/I_c = 0.9$ and at (b) $I_{op}/I_c = 1.19$. Each square in the 2D representation of the cylindrical coordinate system represents a turn of the winding. Only one value of power is assigned to each turn at a given I_{op}; for the sake of representation, a shading color plot is obtained via 2D interpolation. At $I_{op}/I_c = 0.9$, the heat generation is concentrated in the third layer, at the upper part of the coil, but the inhomogeneities are still limited below 20% (see Fig. 5a). A much greater dissipated power is obtained for $I_{op}/I_c = 1.2$ (see Fig. 5b), since I_{op} is higher and the current is above critical. The heat generation mainly occurs in the regions close to the connections of the coil to the current leads. In these regions, the power per unit length is more than 3 times greater than at the turns of the 3rd layer at the bottom of the winding.

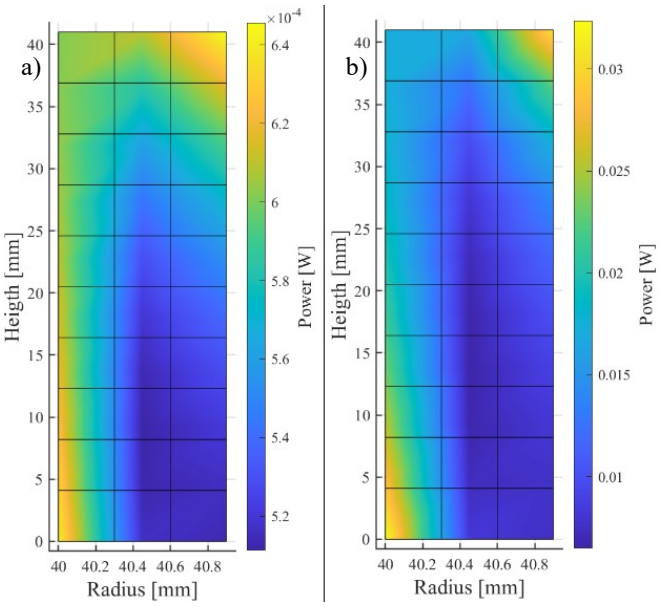

Fig. 5. Dissipated power generated in the turns of the NI coil during the charging phase, at (a) $I_{op}/I_c = 0.9$ and at (b) $I_{op}/I_c = 1.19$, obtained with the numerical model.

V. Conclusion

The electrical characteristics of two BSCCO coils realized with the layer-wound technique were measured. The measurements on the insulated coil show, as expected, similar voltage traces in the various layers, with discrepancies which can be ascribed to the difference of critical current in the various layers. The voltages measured on the non-insulated coil reveal instead a clear difference in the time evolution of the voltage of the outer layers with respect to the inner one.

In order to interpret these results, a lumped parameter nonlinear electric circuit model of the coil was developed, which allows interpreting the voltage development in the various layers in terms of the current redistribution inside the winding during the transport current ramp. At the ramp rate level adopted (1 A/s), the currents flowing in radial direction in the NI coil are driven by inductive effects for transport currents up to 40% of the critical current, and by resistive effects for transport currents above 80 % of the critical one.

The model reveals that the most stressed turns in terms of power dissipation in this layer-wound coil are those located in proximity of the current leads.

REFERENCES

[1] S. Hahn *et al., "HTS pancake coils without turn-to-turn insulation," IEEE Trans. Appl. Supercond*., vol. 21, no. 3, pp. 1592–1595, Jun. 2011.

[2] S. B. Kim *et al., "The normal-zone propagation properties of the non-insulated HTS coil in cryocooled operation," Phys. C, vol*. 471, pp. 1428–1431, May 2011.

[3] S. Hahn *et al., "'Defect-irrelevant' behavior of a no-insulation pancake coil wound with REBCO tapes containing multiple defects," Supercond. Sci. Technol*., vol. 29, p. 105017, Sept. 2016.

[4] K. R. Bhattarai *et al., "Quench Analysis of a Multiwidth No-Insulation 7-T 78-mm REBCO Magnet," IEEE Trans. Appl. Supercond.*, vol. 27, no. 4, p. 4603505, Jun. 2017.

[5] M. Cho *et al., "Combined Circuit Model to Simulate Post-Quench Behaviors of No-Insulation HTS Coil," IEEE Trans. Appl. Supercond.*, vol. 29, no. 5, p. 4901605, Aug. 2019.

[6] H. W. Weijers *et al., "High Field Magnets With HTS Conductors," IEEE Trans. Appl. Supercond*., vol. 20, no. 3, pp. 576–582, Jun. 2010.

[7] Y Suetomi *et al., "Mechanism of notable difference in the field delay times of no-insulation layer-wound and pancake-wound REBCO coils," Supercond. Sci. Technol.*, vol. 29, no. 10, p. 105002, Aug. 2016.

[8] S. Choi *et al., "A Study on the No Insulation Winding Method of the HTS Coil," IEEE Trans. Appl. Supercond*., vol. 22, no. 3, p. 4904004, Jun. 2012.

[9] K. Yanagisawa *et al., "A Long Charging Delay for a No-Insulation REBCO Layer-Wound Coil and Its Influence on Operation With Outer LTS Coils," IEEE Trans. Appl. Supercond*., vol. 26, no. 6, p. 4602304, Feb. 2019.

[10] D. Liu *et al., "Numerical analysis of thermal stability and mechanical response in a no-insulation high-temperature superconducting layer-wound coil," Supercond. Sci. Technol.*, vol. 32, p. 044001, Aug. 2016.

[11] Y Suetomi et al., "*A novel winding method for a no-insulation layer-wound REBCO coil to provide a short magnetic field delay and self-protect characteristics," Supercond. Sci. Technol*., vol. 32, p. 045003, Feb. 2019.

[12] T. Wang *et al., "Analyses of Transient Behaviors of No-Insulation REBCO Pancake Coils During Sudden Discharging and Overcurrent*," *IEEE Trans. Appl. Supercond*., vol. 25, no. 3, p. 4603409, Jun. 2015.

[13] H. Song and Y. Wang, "*Simulations of Nonuniform Behaviors of Multiple No-Insulation (RE)Ba2Cu3O7-x HTS Pancake Coils During Charging and Discharging," IEEE Trans. Appl. Supercond*., vol. 26, no. 4, p. 4700105, Jun. 2015.

[14] X. Wang *et al., "Charging Behavior in No-Insulation REBCO Pancake Coils," IEEE Trans. Appl. Supercond.,* vol. 25, no. 3, p. 4601805, Jun. 2015.

[15] T. Oki *et al., "Evaluation on Quench Protection for No-Insulation REBCO Pancake Coil," IEEE Trans. Appl. Supercond.,* vol. 26, no. 4, p. 4702905, Jun. 2016.

[16] X. Wang *et al., "Turn-to-turn contact characteristics for an equivalent circuit model of no-insulation ReBCO pancake coil," Supercond. Sci. Technol*., vol. 26, p. 035012, Jan. 2013.

[17] S. Noguchi *et al., "Turn-to-Turn Contact Resistance Measurement of No-Insulation REBCO Pancake Coils," IEEE Trans. Appl. Supercond*., vol. 29, no. 5, p. 4601605, Aug. 2019.

[18] Y. Kakimoto *et al., "Evaluation of Electromagnetic Behavior of No-Insulation REBCO Pancake Coil With Multiple Defects," IEEE Trans. Appl. Supercond*., vol. 29, no. 5, p. 4603005, Aug. 2019.

[19] S. Hahn *et al., "No-Insulation Coil Under Time-Varying Condition: Magnetic Coupling With External Coil," IEEE Trans. Appl. Supercond.*, vol. 23, no. 3, p. 4601705, Jun. 2013.

[20] M. Xu *et al.,* "*Experimental Layer-Wound Mock-Up Coil for HTS MRI Magnet Using BSCCO Tape," IEEE Trans. Appl. Supercond*., vol. 19, no. 3, p. 2309, Jun. 2009.

[21] M. Breschi, *et al. "Dependence of Critical Current and Quench Energy of BSCCO-2223 Tapes on Bending Diameter," IEEE Trans. on Appl. Supercond*., vol. 26, n. 3, p. 8000605, Feb. 2016.

[22] https://www.amsc.com/

[23] M. Wilson, *"Superconducting Magnets,"Oxford Science Publ., Clarendon Press*, Mar. 1987.

[24] G. Liu *et al., "Experimental and numerical study of frequency-dependent transport loss in YBa 2 Cu 3 O 7–δ coated conductors with ferromagnetic substrate and copper stabilizer," J. Appl. Phys*., vol. 121, no. 24, p. 243902, Jun. 2017.

[25] W. H. Hayt and J. E. Kemmerly, "*Engineering Circuit Analysis (5th Ed.)," New York: McGraw Hill,* 1993.

[26] J. R. Cash and A. H. Karp, "*A variable order Runge-Kutta method for initial value problems with rapidly varying right-hand sides," Trans. On Math. Softw.*, vol. 16, no.3, pp. 201–222, Sept. 1990.

[27] S. C. Wimbush and N. M. Strickland, "*A Public Database of High-Temperature Superconductor Critical Current Data," IEEE Trans. Appl. Supercond*., vol. 27, no. 4, p. 8000105, Jun. 2017.

[28] Z. Ni *et al., "Globally Optimal Algorithm for Design of 0.7 T Actively Shielded Whole-Body Open MRI Superconducting Magnet System," IEEE Trans. Appl. Supercond.*, vol. 23, no. 3, p. 4401104, Jun. 2013.

[29] Q. Wang *et al., "Design and Test of Conduction-Cooled High Homogenous Magnetic Field Superconducting Magnet for Gyrotron," IEEE Trans. Appl. Supercond.*, vol. 17, no. 2, p. 2319, Jun. 2007.